

# Exploring the Changes in the Structure of $\alpha$ -Helical Peptides Adsorbed onto a Single Walled Carbon Nanotube Using Classical Molecular Dynamics Simulation

K. Balamurugan, R. Gopalakrishnan, S. Sundar Raman, and V. Subramanian\*

Chemical Laboratory, Central Leather Research Institute, Council of Scientific and Industrial Research, Adyar, Chennai- 600020, India

Received: July 5, 2010; Revised Manuscript Received: August 27, 2010

Classical molecular dynamics (MD) simulation has been carried out in an explicit solvent environment to understand the interaction between the single walled carbon nanotube (SWCNT) and  $\alpha$ -helix. A polyalanine peptide consisting of 40 alanine residues has been chosen as the model for the  $\alpha$ -helix ( $PA_{40}$ ). Results reveal that the SWCNT induces conformational changes in  $PA_{40}$ . Furthermore, breakage of hydrogen bonds in the chosen model peptides has been observed, which leads to conformational transitions ( $\alpha \rightarrow$  turns) in different parts of the  $PA_{40}$ . Owing to these transitions, regions of different structural and energetic stability are generated in  $PA_{40}$  which enable the  $PA_{40}$  to curl around the surface of the SWCNT. The overall observations obtained from the MD simulations are not significantly influenced by the starting geometry and the choice of the force field. Although the qualities of structural information obtained from the MD simulation using ff03 and OPLS are different, the overall observation derived from the ff03 is similar to that of OPLS. Results from the MD simulation on the interaction of the  $\alpha$ -helical fragment of the SNARES protein with the SWCNT elicit that the amino acid composition influences the interaction pattern. The wrapping of the  $\alpha$ -helical fragment of the SNARES onto the SWCNT is similar to that of  $PA_{40}$ . Overall, there is a considerable decrease in the helical content of peptides upon interaction with SWCNTs, in agreement with the experimental findings.

## 1. Introduction

SWCNTs have drawn significant attention due to their potential applications in nanoelectronics, material science, molecular detection, and nanobiotechnology.<sup>1–6</sup> However, the applications of SWCNTs are limited due to their high hydrophobic nature, which leads to uncontrolled aggregation of SWCNTs in an aqueous solution. Owing to this problem, it is very difficult to assemble SWCNTs into useful structures. To realize various applications of SWCNTs, a plethora of functionalization is being developed using organic, inorganic, and biological macromolecules. The functionalization of SWCNTs using biomolecules has gained importance due to their wide-ranging applications in nano biotechnology, biosensors, biomedical devices, drug delivery systems, artificial muscles, and cellular delivery of peptides and proteins.<sup>7–10</sup> From the nanobiotechnology viewpoint, the structure and function of the enzymes adsorbed on SWCNTs have been investigated.<sup>11</sup> It is found from the previous investigation that soybean peroxidase activity reduced up to 30% of its native activity upon its adsorption to a SWCNT while adsorbed  $\alpha$ -chymotrypsin exhibited only 1% of its native activity.<sup>11</sup> The reduction of the activity is due to changes in the secondary structure of the protein upon adsorption onto a SWCNT. Particularly,  $\alpha$ -chymotrypsin undergoes substantial changes upon its interaction with a SWCNT. Recent experimental reports on the adsorption of BSA onto a SWCNT disclosed that there are considerable changes in the secondary structures of BSA.<sup>12,13</sup> Particularly, significant reduction in the  $\alpha$ -helical content has been observed. However, the explanation for the observed structural changes is yet to be put forwarded.<sup>12,13</sup> In addition to the proteins, the interaction of amphiphilic  $\alpha$ -helical peptide (Nano1) with a

SWCNT has been probed using both experimental and MD simulation studies. It is found that the stacking interaction of aromatic amino acid with the SWCNT plays a crucial role in the stabilization of the intermolecular complex.<sup>14,15</sup>

The uses of SWCNT-based materials under in vivo conditions calls for further investigation to understand how SWCNTs induce conformational changes in the proteins and nucleic acids structure. The information obtained from these studies would be useful to gain insight into the forces involved in SWCNT–biomolecule interactions, which helps researchers design new biocompatible materials. In this context, molecular dynamics (MD) simulation is one of the attractive tools that can be successfully used to probe the interaction between the biomolecules and SWCNTs. The three-dimensional structure of the proteins is made up of secondary structural elements like helix, sheet, strands, loops, and turns. The combination of these structural elements form super secondary motifs like  $\alpha$ – $\alpha$ ,  $\beta$ – $\alpha$ – $\beta$ , and  $\beta$ -hairpins.<sup>16</sup> The helix is one of the most frequently occurring secondary structures in the protein. The length of the helix varies from few residues to 50 residues. The longer helices are present in proteins like fibrinogen and membrane proteins. The helical motifs can adopt any of the conformations such as  $3_{10}$ -helix,  $\alpha$ -helix, and  $\pi$ -helix. The  $3_{10}$ -helix,  $\alpha$ -helix, and  $\pi$ -helix are characterized by the consecutive  $(i, i + 3)$ ,  $(i, i + 4)$ , and  $(i, i + 5)$  hydrogen bonds, respectively. The  $\alpha$ -helix and  $3_{10}$ -helix are commonly found in proteins.<sup>17</sup> Among these two helices, the  $\alpha$ -helix is the most predominantly observed secondary structural element and it is more stable than that of the  $3_{10}$ -helix.<sup>17</sup>

Several experimental and theoretical studies have been made on the sequence, structure, stability, and dynamics of helices.<sup>18–23</sup> Since there is a huge volume of literature on this topic, some of the recent contributions are only highlighted.<sup>24–28</sup> The hydrogen-bonding (H-bonding) interactions in  $\alpha$ -helical poly-

\* To whom correspondence should be addressed. Tel: +91 44 24411630. Fax: +91 44 24911589. E-mail: subuchem@hotmail.com, subbu@clri.res.in.

**TABLE 1: Details of Various Systems Simulated in This Study**

system name	force field	description	box dimension	no. of water molecules
PA <sub>40</sub> (ff03)	Amber ff03	PA <sub>40</sub>	6.0 × 6.0 × 8.0	9460
PA <sub>40</sub> (OPLS)	OPLS	PA <sub>40</sub>	6.0 × 6.0 × 8.0	9460
SWCNT-PA <sub>40</sub> (ff03)	Amber ff03	PA <sub>40</sub> aligned parallel to the SWCNT at about 8.5 Å distance	6.0 × 6.0 × 9.12	10347
SWCNT-PA <sub>40</sub> (OPLS)	OPLS	PA <sub>40</sub> aligned parallel to the SWCNT at about 8.5 Å distance	6.0 × 6.0 × 9.12	10347
SWCNT-PA <sub>40</sub> Angular(OPLS)	OPLS	PA <sub>40</sub> aligned ~45° to the axis of the SWCNT at about 8.5 Å distance	6.0 × 6.0 × 9.12	10363
SWCNT-SNARE(OPLS) (PDB ID: 1scf CHAIN H 140–199)	OPLS	SNARE peptide aligned parallel to the SWCNT at about 10 Å distance	6.0 × 6.0 × 12.46	14113

alanine peptide have been quantified using the theory of atoms in molecule (AIM).<sup>24</sup> Previous experimental study has shown that an increase in the sequence length of alanine peptide favors α-helix over 3<sub>10</sub>-helix<sup>25</sup> and longer alanine based peptides form a stable α-helix.<sup>26–28</sup> Earlier molecular dynamics study on the polyalanine (PA) peptide shows that the helical content of the peptide remains almost constant when its length ranges from 10 to 40 residues.<sup>29</sup> On the basis of these findings PA<sub>40</sub> has been selected as the model peptide for the α-helix. Furthermore, due to the higher hydrophobic index of the alanine, it serves as a good model for the hydrophobic system. The hydrophobic–hydrophobic interaction is the major driving force for the self-assembly of nonpolar solutes in aqueous solutions. The importance of hydrophobic interaction in biological as well as synthetic systems, including supramolecular systems has been well documented.<sup>30–33</sup> Thus studies on the interaction between the α-helix and SWCNT forms a valuable model for the hydrophobic–hydrophobic interaction in biological systems.

Although several molecular dynamics simulations have been reported on the conformation and energy landscape of an α-helix employing different force field parameters, the issues pertaining to the reliability of various force fields to predict appropriate α-helical conformation of the chosen peptide is still not resolved.<sup>34–37</sup> Recently, Matthes et al. have shown that AMBER ff03 parameters overstabilize the helix conformation of the Fs<sub>21</sub> (21 residue polyalanine peptide) peptide whereas the OPLS force field (OPLS-AA/L hereafter shortly called as OPLS) predicts helix content comparable to that of the experimental CD spectra. The same study has also revealed that ff99sb parameters do not yield helical conformation for the Fs<sub>21</sub> peptide.<sup>38</sup> On the basis of the above-mentioned study, we have selected ff03 and OPLS force field parameters for the present investigation.

In this study, an attempt has been made to investigate how an α-helix interacts with the SWCNT using classical MD simulation in an explicit solvent environment. In addition, the results obtained from the MD simulation on the SWCNT–α-helical model peptide have also been compared with that of an α-helical peptide derived from the soluble *N*-ethylmaleimide-sensitive factor attachment protein receptor (SNARE). The effects of the SWCNT on the α-helical conformation and the part played by the amino acid sequence composition of the SNARE peptide have also been discussed.

## 2. Computational Details

MD simulations are widely used to study the protein structure, function, and interaction.<sup>39–41</sup> Classical MD simulations have also been carried out on SWCNTs and their interaction with proteins, nucleic acids, and synthetic polymers.<sup>14,42–47</sup> In this study, full atomistic MD simulations on SWCNT-PA<sub>40</sub>, SWCNT-SNARE, and PA<sub>40</sub> systems were performed.

**2.1. Construction of Models.** **2.1.1. SWCNT.** A SWCNT with chirality (6,6) and length ~89.6 Å was built using the VMD Package (<http://www.ks.uiuc.edu/Research/vmd/>),<sup>48</sup> which con-

sists of 888 carbon atoms and the same was used to probe the interaction with the PA<sub>40</sub> system. Another SWCNT of same chirality of length ~119.1 Å consisting of 1176 carbon atoms was used to understand the interaction with SNARE peptide. To simulate an infinite SWCNT, a segment with length equal to the L<sub>z</sub> box dimension was aligned along the z-axis with the terminal carbons sharing a chemical bond. On the basis of previous work of Hummer et al., SWCNT atoms were modeled as uncharged Lennard-Jones particles using sp<sup>2</sup> carbon parameters of the respective force field.<sup>49</sup> The choice of uncharged carbon atoms for the SWCNT was also justifiable from the recent study of Jordan and co-workers.<sup>50</sup> They considered extended π-systems as the models for the graphite. In that study, the interaction of water molecule with coronene and dodeca-benzocoronene was investigated. They showed that as the size of the π-systems increase, the charge on the carbon atoms decreases; in fact, it vanishes on the inner carbon atoms with increasing ring size.<sup>50</sup> Further, it was found that dispersion interaction plays the dominant role when compared to that of electrostatic interaction in the stabilization of extended π-system–water intermolecular complex.<sup>50</sup>

**2.1.2. PA<sub>40</sub>.** The PA<sub>40</sub> with its ends capped by acetyl (ACE) and *N*-methylamine (NME) groups was built in α-helix conformation using PyMol.<sup>51</sup> The length of the helix is ~54 Å. The initial peptide conformation was set to perfectly α-helix with backbone dihedral angles of φ = -57° and Ψ = -47°.

**2.1.3. SNARE.** It is a membrane protein predominantly composed of α-helices (~75%). The initial geometry of the protein was taken from the crystal structure of the neuronal SNARE complex at 2.4 Å resolution (PDB ID 1SFC).<sup>52</sup> One of the α-helices of the protein (from sequence no. 141–199) present in the H chain of the SNARE protein was taken as the model for the α-helix in a real life system.

**2.2. Models.** Different model systems considered in this study are (i) PA<sub>40</sub>(ff03),<sup>53</sup> (ii) PA<sub>40</sub>(OPLS),<sup>54,55</sup> (iii) SWCNT-PA<sub>40</sub>(ff03), (iv) SWCNT-PA<sub>40</sub>(OPLS), and (v) SWCNT-PA<sub>40</sub>Angular(OPLS). The force fields used to perform MD simulations are indicated in parentheses. In models (iii) and (iv), the center of mass of the peptide was initially placed 8.5 Å away from the side wall of the SWCNT and PA<sub>40</sub> was aligned parallel to the length of the SWCNT, as described in the previous study.<sup>14</sup> In the fifth model, the center of mass of the peptide was initially placed 8.5 Å away from the side wall of the SWCNT and PA<sub>40</sub> was aligned ~45° to the length of the SWCNT. In addition, another model system was built using the helical peptide from the SNARE protein. It is designated as SWCNT-SNARE(OPLS). In this model, the helical peptide was initially placed 10 Å away from the side wall of the SWCNT and it was aligned parallel to the length of the SWCNT. The counterions were added (five Na<sup>+</sup> ions) to neutralize the system. The above-mentioned nomenclatures are used in the remaining of the manuscript. All the systems were solvated with SPC water.<sup>56</sup> The box size and number of water molecules present

in the various systems were given in Table 1. MD simulations were performed using the GROMACS 4.0.7 package (<http://www.gromacs.org/>).<sup>57–59</sup> The van der Waals interaction and the CH–π interaction play an important role in the interaction process between the SWCNT and PA<sub>40</sub>. These interactions were parametrized within the van der Waals parameters of each atom type in the force fields. It is found from the recent study that the qualitative description of CH–π interaction is feasible with the help of both ff03 and OPLS force fields.<sup>60</sup> This evidence clearly shows that the above-mentioned force fields are suitable for modeling the SWCNT–helical peptide systems.

All simulations were carried out in the isothermal–isobaric (NPT) ensemble with periodic boundary conditions applied in three dimensions. The pressure was controlled at 1 atm and the temperature was retained at 300 K using a Parrinello–Rahman barostat and V-rescale thermostat, respectively.<sup>61–63</sup> A 2 fs time step was used to integrate the equation of motion. The electrostatic interaction was calculated using particle mesh Ewald sums with a nonbonded cutoff of 10 Å.<sup>64</sup> Bonds between hydrogen and heavy atoms were constrained at their equilibrium length using the LINCS algorithm.<sup>65</sup> The positions of SWCNT atoms were constrained with a harmonic potential. Various steps involved in the simulation were minimization of the whole system, solvent equilibration by restraining both the SWCNT and peptide for 1 ns, and the equilibration of the whole system for 300 ps. The analysis of the energy parameters revealed that the system was found to be well equilibrated. Then production runs of 10 ns were carried out for all the systems. The trajectories were saved at a 1 ps interval for further analysis. The analysis of the trajectories was made using the GROMACS suite of programs.<sup>57–59</sup> The results were visualized using the VMD package.<sup>48</sup> Various parameters derived from the simulations are described in the following section.

### 3. Analysis

**3.1. Root-Mean-Square Deviation (RMSD).** RMSD of the peptides was calculated with respect to initial conformation as a function of time using eq 2.

$$\text{RMSD}(t) = \left[ \frac{1}{N} \sum_{i=1}^N \left\| \mathbf{r}_i(t) - \mathbf{r}_i(0) \right\|^2 \right]^{1/2} \quad (1)$$

where  $\mathbf{r}_i(t)$  represents the position of atom  $i$  at time  $t$  and the same is compared with the  $\mathbf{r}_i(0)$  position of the atom at time zero and  $N$  is the total number of backbone atoms.

**3.2. Secondary Structure Analysis.** The secondary structure analysis of the peptide was calculated using the DSSP (dictionary of protein secondary structure: pattern recognition of hydrogen-bonded and geometrical features) protocol available in the do\_dssp module of the Gromacs package.<sup>66</sup> In this protocol, hydrogen-bonding and other geometrical parameters were used to assign the secondary structures of the peptide.

**3.3. Helical Fraction.** Apart from the terminal acetyl (ACE) and *N*-methylamine (NME) residues, only 38 residues are in the α-helical conformation in PA<sub>40</sub>. These residues were considered for the analysis. The helical fraction of the PA<sub>40</sub> was calculated by counting the number of residues in α-helical conformation divided by 38, which generates a value between 0 and 1.

**3.4. Hydrogen Bond Analysis.** Hydrogen-bonding interactions in α-helical conformation were calculated from eq 2,

$$H_i = \begin{cases} 1, & ((d(H_i \cdots O_i) \leq 3.5 \text{ \AA}) \text{ and} \\ & (120^\circ \text{ angle } (O_i \cdots H_i - N_i) \leq 180^\circ)) \\ 0, & \text{otherwise} \end{cases} \quad (2)$$

where H<sub>i</sub> is the possible *i*th intramolecular hydrogen bond in the α-helix. The number of hydrogen bonds present in the α-helix as a function of time was calculated from the trajectory.

**3.5. Contact Area.** The area of the molecular surface buried in contact between the two macromolecules is called the interface area or contact area of the molecular assembly. It was calculated as

$$\text{contact area} = \frac{1}{2}((\text{SAS}_{\text{pep}} + \text{SAS}_{\text{SWCNT}}) - \text{SAS}_{\text{complex}}) \quad (3)$$

where SAS<sub>pep</sub> and SAS<sub>SWCNT</sub> are the solvent accessible surface area of the isolated peptide and SWCNT, respectively, and SAS<sub>complex</sub> is that of the whole assembly of the SWCNT and peptide.

**3.6. Cluster Analysis.** Cluster analysis was performed using the GROMOS method.<sup>67</sup> This method was shown to be effective for judging the convergence of MD simulations. Structures of the protein were taken from the MD trajectory at 10 ps intervals. The matrix of atom positional root-mean-square deviations between pairs of structures was calculated for both the SWCNT

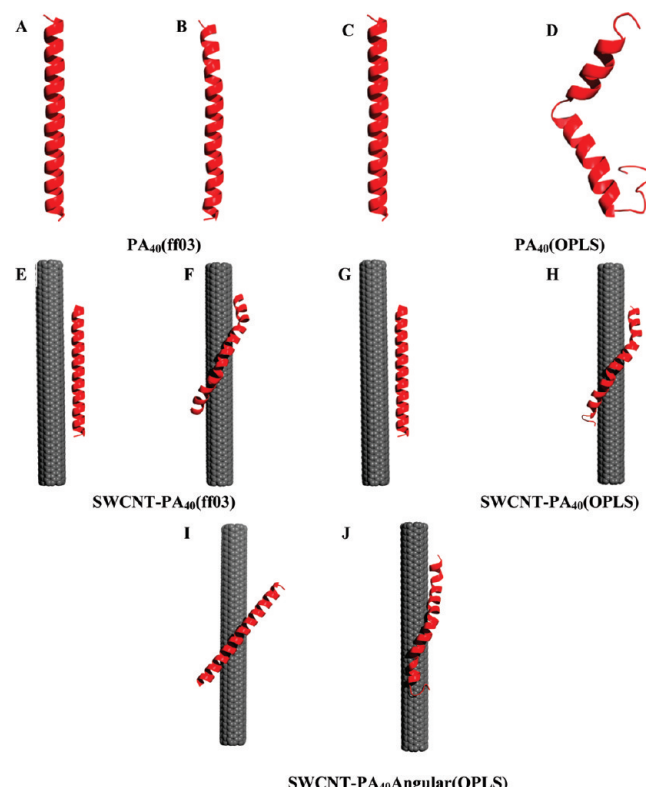


**Figure 1.** Representative structures of SWCNT-PA<sub>40</sub> from the MD simulations. (A) and (B) are the initial and final conformations of the PA<sub>40</sub>(ff03) system, (C) and (D) are the initial and final conformations of the PA<sub>40</sub>(OPLS) system, (E) and (F) are the initial and final conformations of the SWCNT-PA<sub>40</sub>(ff03) system, (G) and (H) are the initial and final conformations of the SWCNT-PA<sub>40</sub>(OPLS) system, and (I) and (J) are the initial and final conformations of the SWCNT-PA<sub>40</sub>Angular(OPLS) system. The SWCNTs are shown as the vdW model and the peptides are represented as the cartoon representation.

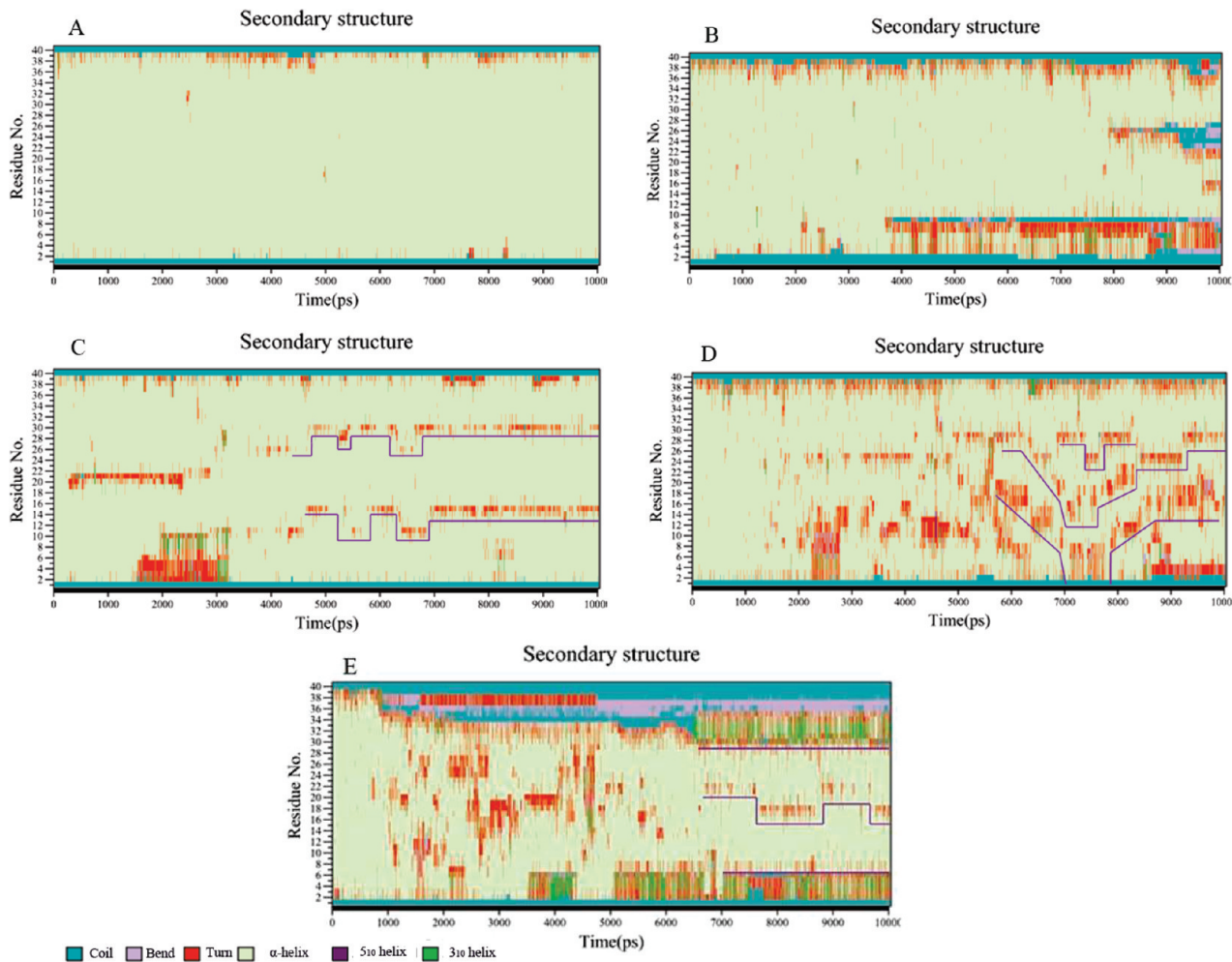


**Figure 2.** Secondary structure assignment of the protein (DSSP) as a function of time for 10 ns: (A) PA<sub>40</sub>(ff03); (B) PA<sub>40</sub>(ff03); (C) SWCNT-PA<sub>40</sub>(ff03); (D) SWCNT-PA<sub>40</sub>(OPLS); (E) SWCNT-PA<sub>40</sub>Angular(OPLS). The violet color line is used to denote the regions of  $\alpha$ -helical breakage.

and peptide residues. The criterion of similarity for two structures belonging to the same cluster was fixed to be RMSD  $\leq 0.50$  nm. The convergence of a simulation was considered to be achieved when the plot of number of clusters as a function of time reaches a plateau.

#### 4. Results and Discussion

**Peptide Conformational Analysis.** The main objective of this investigation is to gain insight into the structure and spatial orientation of the helical peptide noncovalently adsorbed onto the SWCNT. Thus various parameters that yield information on these features are derived from the trajectories of SWCNT-PA<sub>40</sub> and PA<sub>40</sub> systems. The most important issue is to understand what kind of conformational changes are induced by the SWCNT on the  $\alpha$ -helix. In this context, it is necessary to quantify the conformational changes in the isolated helical peptide (in the absence of a SWCNT) during the MD simulation. It has been shown that the ff03 parameters slightly overstabilize the helix whereas the OPLS parameters yield results comparable to that of experimental values.<sup>38</sup> Thus it is pertinent to evaluate the role of force field parameters in yielding the stable helical conformation. Therefore, MD simulations have been carried out on the isolated model of helical peptide using both force field parameters.

Figure 1 shows the initial arrangement and final snapshot for different model systems. It can be seen from the Figure 1

(A–D) that both ff03 and OPLS force field parameters predict a helical structure for the model peptide with different helical contents. It is evident from Figure 1D that the OPLS force field parameters yield a small amount of helical unwinding. However, there are no drastic changes in the helical conformation of the chosen model peptide.

Figure 1(E–J) elicits that the  $\alpha$ -helix partially wraps around the surface of the SWCNT. The comparison of the results obtained for the isolated helical peptide with that of the SWCNT-PA<sub>40</sub> system explains that conformational changes in the helical peptide are mainly due to the interaction between the two systems and as a consequence the model peptide wraps around the SWCNT.

It is found from the simulation that due to the interaction of helical peptide with the SWCNT, small helical fragments are generated. These helical fragments facilitate the wrapping of the peptide on to the surface of the SWCNT. It can be noted from the results that both force field parameters yield similar trends in the fragmentation of the helix upon its interaction with the SWCNT.

It is well-known that the results of the MD simulation depend on the starting geometry of the system. Hence, simulations were performed for two different starting arrangements: (i) helical peptide is placed parallel to the long axis of the SWCNT and (ii) the same peptide is aligned at an angle of  $\sim 45^\circ$  to the long axis of the SWCNT. Parts I and J of Figure 1 are the initial

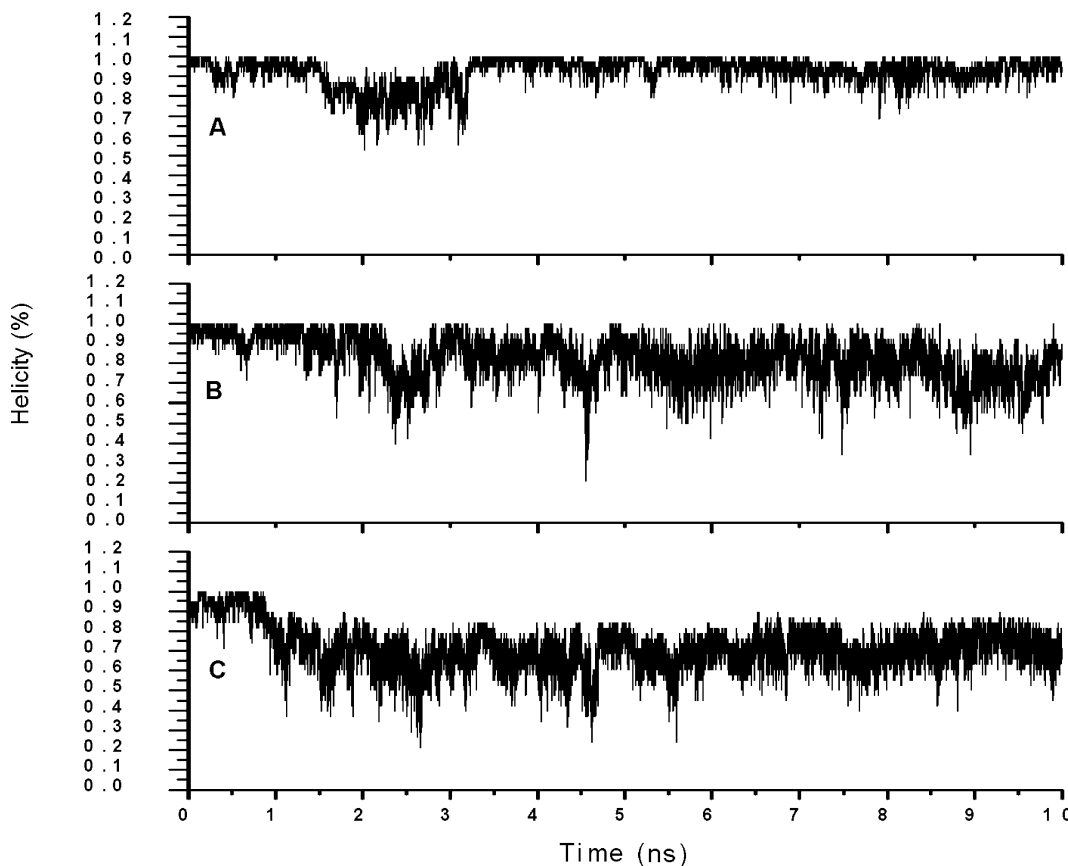


**Figure 3.** Helical fraction of the SWCNT-PA<sub>40</sub> systems as a function of time: (A) SWCNT-PA<sub>40</sub>(ff03); (B) SWCNT-PA<sub>40</sub>(OPLS); (C) SWCNT-PA<sub>40</sub>Angular(OPLS).

arrangements and final conformation obtained from the MD simulation for the SWCNT-PA<sub>40</sub> Angular(OPLS) system. The final snapshots extracted from the MD trajectory are given in (H) and (J) of Figure 1, which show that the PA<sub>40</sub> tends to wrap onto the SWCNT irrespective of the initial arrangement. It is evident that there are no significant differences in the wrapping patterns due to the differences in the starting arrangement. Further evidence shows that these findings are independent of their starting arrangements and choice of the force field parameters.

The changes in the helical conformation upon interaction with the SWCNT have been obtained from the DSSP protocol. The variations in the secondary structure with respect to time are plotted in Figure 2. It is observed from Figure 2A that the ff03 force field predicts an  $\alpha$ -helix for the PA<sub>40</sub> throughout the simulation period except for deviations in the terminal residues. Figure 2B represents the secondary structure plot of the PA<sub>40</sub> obtained from the simulation using the OPLS force field. It can be noticed that a break in the helical structure occurs at the eighth nanosecond of the simulation due to the inherent nature of the OPLS force field. In addition, these parameters cause flanking of terminal residues. These findings have clearly revealed the differences in the modeling of helical peptides using different force fields. However, both force fields yield a relatively stable helix throughout the simulation.

Parts C and D of Figure 2 represent the variations in the secondary structure with time for the SWCNT-PA<sub>40</sub>(ff03) and SWCNT-PA<sub>40</sub>(OPLS) systems, respectively. The results show that the interaction of PA<sub>40</sub> with the SWCNT induces turns in the  $\alpha$ -helical conformation of the peptide at some specified intervals, which divide the full length of the  $\alpha$ -helix into smaller  $\alpha$ -helical fragments. It is interesting to note from the plot that

the regions that have undergone conformational changes are retained throughout the simulation using the ff03 force field. On the other hand, both breakage and formation of helices are observed in the simulation using OPLS force field parameters. The nonhelical regions adopt helical conformation and vis-a-vis helical regions undergo nonhelical transition during the simulation. On the whole,  $\alpha$ -helical fragments are retained throughout the simulation time.

The secondary structure plot for the SWCNT-PA<sub>40</sub>Angular(OPLS) system is displayed in Figure 2E. It can be observed that the SWCNT induces  $\alpha \rightarrow 3_{10}$  helix transition. Further, the large helical peptide is divided into smaller fragments of  $\alpha$  and  $3_{10}$  helices. The interaction of PA<sub>40</sub> with the SWCNT weakens the  $\alpha$ -helical conformation and causes helix breakage at some interval to facilitate the partial wrapping of the helix around the SWCNT. To assess the overall loss in the helicity, the helical fraction of the PA<sub>40</sub> was calculated from the trajectories and the results are given in Figure 3. Approximately 15–30% loss in the overall helicity of the peptide has been observed upon interaction with the SWCNT. Simulations using both the force fields and different starting arrangements provide a similar trend in the overall helicity changes during the interaction. Evidences from DSSP analysis and helical fraction elicit that the loss in helicity is important to facilitate the interaction between the model peptide with the SWCNT. Particularly, the changes in the helical conformation in some intervals maximize the interaction between the two systems.

From the above observation, it is found that the SWCNT causes breakage (kinks) in the structure of the helix. Kumar et al. have carried out a systematic study on the structural and sequence characteristics of  $\alpha$ -helices using a database of 1131  $\alpha$ -helices with nonidentical sequences from 205 nonhomologous

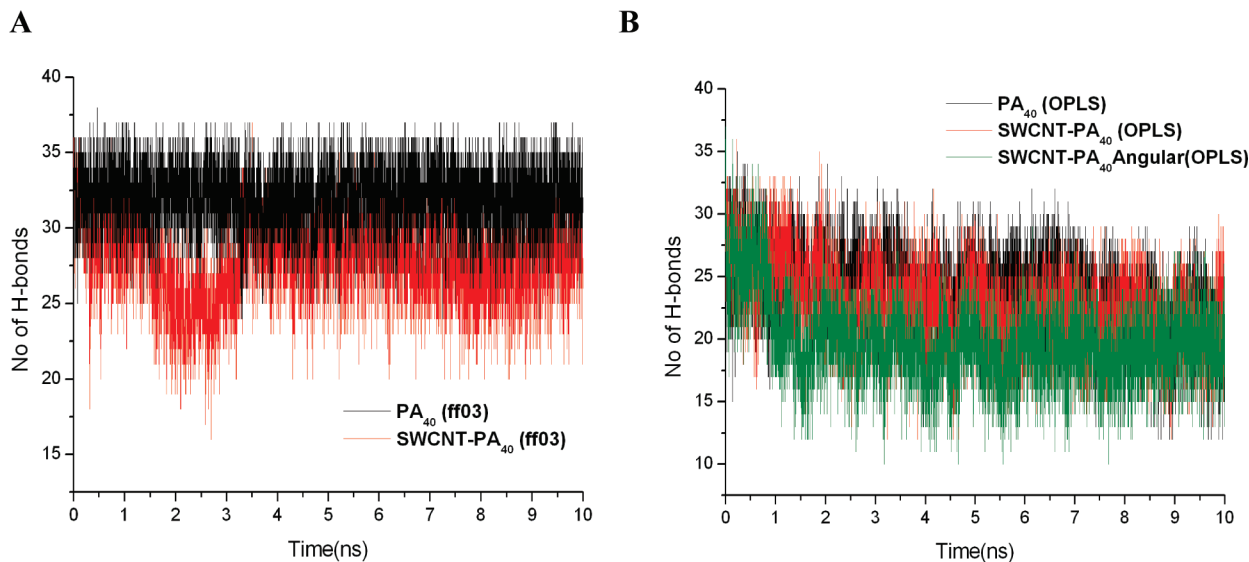


**Figure 4.** Number of H-bonds present in the SWCNT-PA<sub>40</sub> systems during the simulation: (A) PA<sub>40</sub>(ff03) and SWCNT-PA<sub>40</sub>(ff03); (B) PA<sub>40</sub>(OPLS), SWCNT-PA<sub>40</sub>(OPLS), and SWCNT-PA<sub>40</sub>Angular(OPLS).

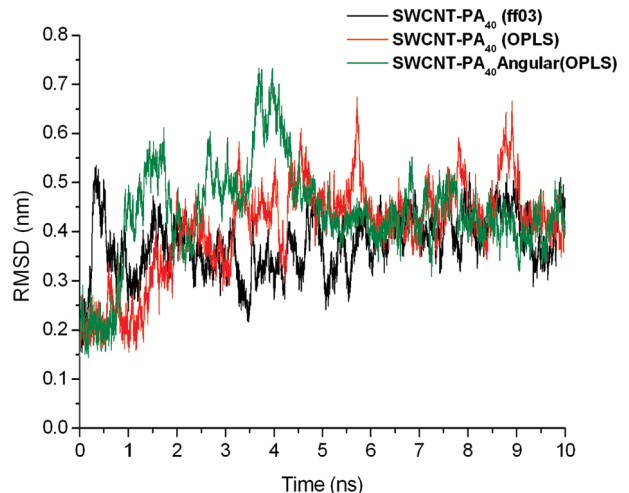


**Figure 5.** Root mean square deviation (RMSD) of the SWCNT-PA<sub>40</sub> systems with respect to their initial structures.

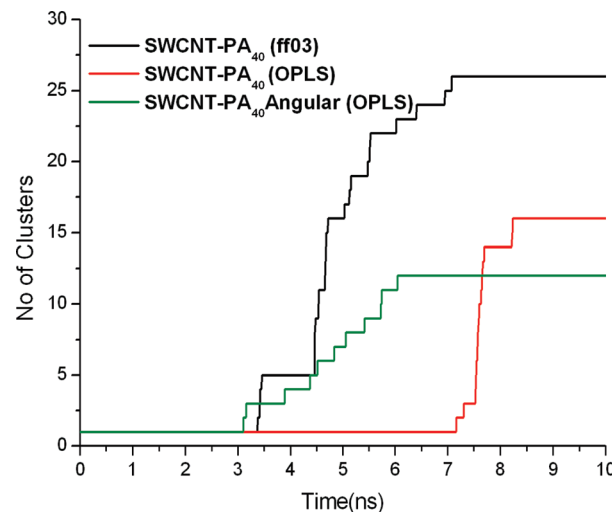


**Figure 6.** Number of clusters obtained from the SWCNT-PA<sub>40</sub> systems as a function of time.

globular protein chains.<sup>68</sup> It was found that as the length of the helix increases, the curvature of the helix decreases.<sup>68</sup> Thus longer helices are generally less curved than shorter ones. They

have determined amino acid specificity for causing kinks in the α-helices. The presence of amino acid proline and glycine in the sequence is majorly responsible for inducing kinks apart from the β-branched residues (Val, Ile, or Thr), aromatic amino acids (Tyr, Trp, or Phe), and His. The comparison of our results and the database analysis further reveals that the probability of forming curved helices by a longer peptide like PA<sub>40</sub> is not possible in the absence of the SWCNT. Moreover, Ala residue does not have the propensity to introduce kink in the longer α-helices. Thus the helix breakage (kink) observed in this study is mainly due to the interaction of the SWCNT with the α-helix.

**4.2. Hydrogen Bonding.** It is found that the interaction of the SWCNT with PA<sub>40</sub> leads to the breakage of the helix. It is well-known that the α-helical structure is completely orchestrated by the backbone hydrogen-bonding interaction. The variations in the number of hydrogen bonds present in the models with time are given in Figure 4. Figure 4A shows the number of H-bonds in PA<sub>40</sub>(ff03) and SWCNT-PA<sub>40</sub>(ff03). The number of H-bonds in the PA<sub>40</sub>(OPLS), SWCNT-PA<sub>40</sub>(OPLS), and SWCNT-PA<sub>40</sub>Angular(OPLS) systems are presented in Figure 4B. It is evident from the illustrations that there is a reduction in the number of hydrogen bonds present in the helix upon interaction with the SWCNT. As a result, the structural stability of the peptide decreases and hence the helix partially curls around the surface of the SWCNT.

**4.3. RMSD and Cluster Analysis.** The RMSD is often used as an indicator of the deviations in the structure from starting geometry with respect to time. The calculated RMSD for SWCNT-PA<sub>40</sub> is given in Figure 5. It can be seen from the results that RMSD increases at a rapid rate from 0 to 5 ns and then it attains saturation. This evidence shows that the system has achieved equilibration and the simulation time is sufficient enough to cover the most probable states.

To assess the conformational saturation, the cluster analysis was performed. The number of clusters as a function of time is shown in Figure 6. The convergence of a simulation can be considered to be achieved if the plot of the number of clusters as a function of time arrives at a constant value. It is observed from the results that in all the systems the number of clusters reaches a plateau in 6–8 ns and afterward there was no further evolution of clusters. The structures of the most dominant cluster

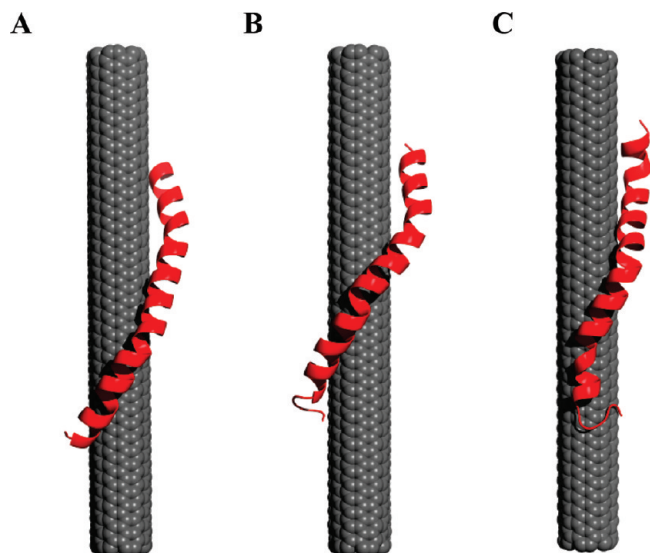


**Figure 7.** Structures of the most dominant cluster extracted from the simulation, (A), (B), and (C) are the dominant structures obtained for SWCNT-PA<sub>40</sub>(ff03), SWCNT-PA<sub>40</sub>(OPLS), and SWCNT-PA<sub>40</sub>Angular(OPLS), respectively.

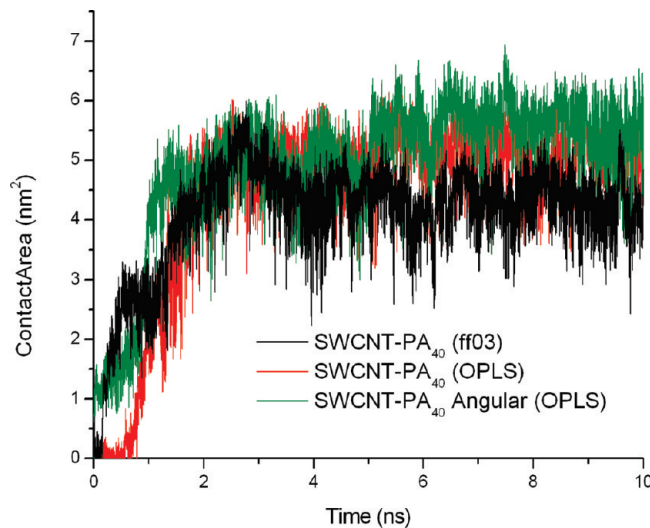


**Figure 8.** Contact area between the SWCNT-PA<sub>40</sub> systems as a function of time.

obtained from the simulation are presented in the Figure 7 which reveals the helical wrapping of the PA<sub>40</sub> onto the SWCNT.

**4.4. Contact Area.** It is well-known that both the SWCNT and PA<sub>40</sub> are hydrophobic in nature. The interaction of the above-mentioned systems in aqueous environment is primarily

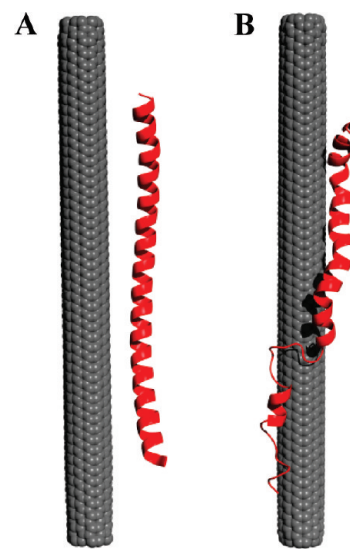


**Figure 10.** Representative snapshot of the SWCNT-SNARE(OPLS) system from the MD simulation. (A) and (B) represents the initial and final conformations, respectively.

driven by hydrophobic–hydrophobic interaction. To quantify the interaction between the two systems, the contact area between the SWCNT and PA<sub>40</sub> was calculated. The results are presented in Figure 8. It can be observed that the contact area rapidly increases for the first two nanoseconds. The variation attains saturation after 6 ns. Afterward there are no significant changes in the contact area with time. The increase in the contact area signifies the removal of water molecule trapped between the systems and the complex formation between the SWCNT and PA<sub>40</sub>.

**4.5. Characterization of the SWCNT-PA<sub>40</sub> Interaction.** The nature of interaction exists between the two systems is characterized using the electrostatic and van der Waals contributions to the total energy. The electrostatic interaction is the primary one in the stabilization of hydrogen bonds present in the helical conformation of the PA<sub>40</sub>. The interaction between the helical peptide and SWCNT predominantly arises from the van der Waals contribution due to the parametrization of carbon atoms in the SWCNT using uncharged Lennard-Jones particles. The above-mentioned energy components of the system are plotted in Figure 9. The results reveal that regardless of the force field and initial geometry, there is a decrease in the electrostatic energy contribution of PA<sub>40</sub> by ~25 kcal/mol. Further there is a gain in van der Waals energy ~75 kcal/mol, as evident from Figure 9. Overall, an energy gain of ~50 kcal/mol is observed during the interaction between the PA<sub>40</sub> and SWCNT. The decrease in the electrostatic energy contribution

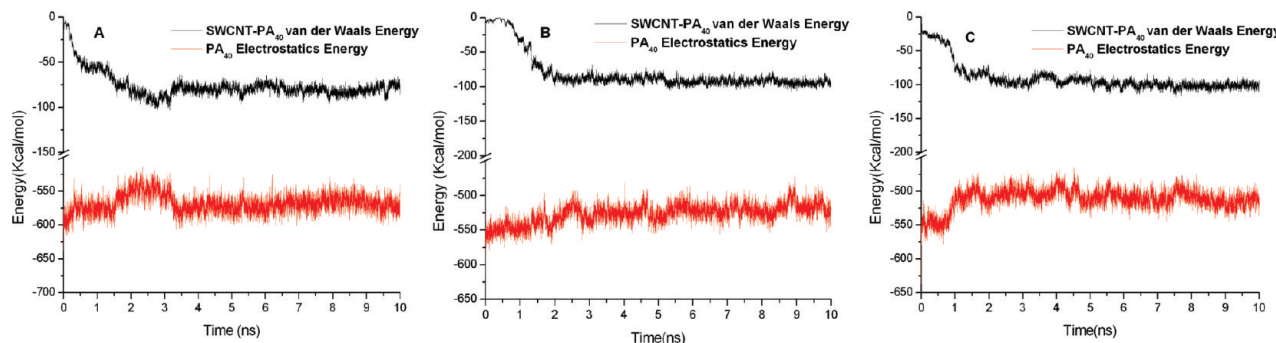


**Figure 9.** van der Waals interaction between the SWCNT-PA<sub>40</sub> system and electrostatic contribution for PA<sub>40</sub> only during the simulation: (A) for SWCNT-PA<sub>40</sub>(ff03); (B) for SWCNT-PA<sub>40</sub>(OPLS); (C) for SWCNT-PA<sub>40</sub>Angular(OPLS).

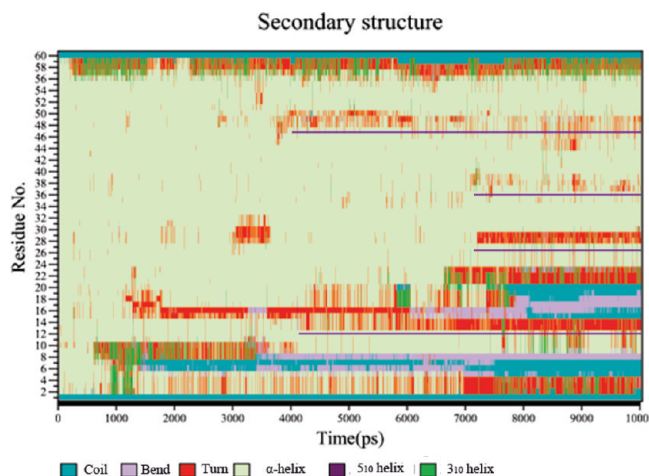


**Figure 11.** Secondary structure assignment of the protein (DSSP) as a function of time for 10 ns for SWCNT-SNARE(OPLS). The violet color line is used to denote the regions of  $\alpha$ -helical breakage.

in the PA<sub>40</sub> is mainly due to the loss of hydrogen bonds in the helix upon its interaction with the SWCNT. The rigidity of the helix is provided by the backbone hydrogen bonds. The breakage of the same increases the flexibility of the helix and decreases the electrostatic energy contribution. As a result, helix is amenable to form kinks that facilitate the interaction process. Thus, the decrease in the electrostatic contribution favors the wrapping of the helix upon the SWCNT.

**4.6. SWCNT-SNARE Complex.** To elucidate how the naturally occurring  $\alpha$ -helical sequence interacts with the SWCNT, a fragment of  $\alpha$ -helix was chosen from the SNARE protein. Figure 10 shows the initial arrangement and final snapshot obtained from the MD simulation on the SWCNT-SNARE complex using the OPLS force field. The secondary structure plot of the SWCNT-SNARE(OPLS) system is given in Figure 11. It can be seen from the results that the helix partially wraps around the SWCNT surface, which is similar to that of the PA<sub>40</sub>. In contrast to PA<sub>40</sub>, the presence of a random coil region (residue nos. 13–22) can be noticed from the results. In the case of the PA<sub>40</sub>, alanine has the highest helix propensity when compared to the other amino acids present in the SNARE. As a result, the changes in the composition in general and helical propensi-

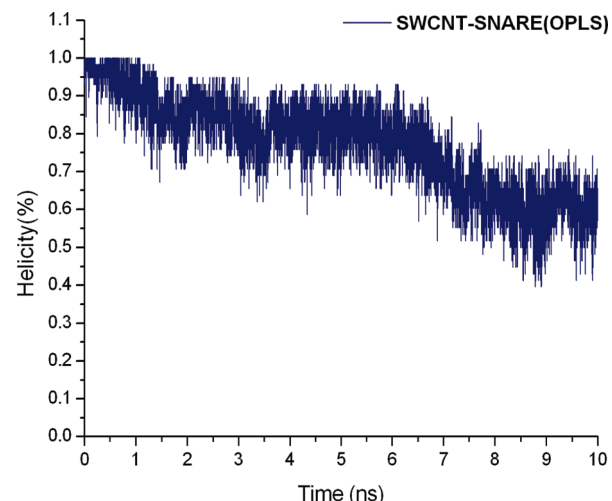


**Figure 12.** Helical fraction of the SWCNT-SNARE(OPLS) systems as a function of time.

ties of different amino acids in particular influence the nature of interaction between the helix and SWCNT. To derive the relationship between the sequence composition and helix breakage, the helix forming tendencies of the fragment of helical motif derived from the SNARES are given in Table 2. It can be seen that alanine has the highest helix propensity whereas the glycine has the lowest helix value.<sup>34</sup> The data shown in Table 2 reveal that the region (from residue nos. 13–22) is composed of amino acids having lesser helix forming propensity when compared to the other regions. Thus this region undergoes conformational transition from helix to random coil upon interaction with a SWCNT. Since glycine can adopt any region in the Ramachandran plot, the presence of same at different positions (17, 20, and 30th positions) in the sequence significantly influences the conformational transitions in the helical motif upon interaction.

The calculated helicity of the SNARE peptide in the presence of a SWCNT is shown in Figure 12. It can be noticed that there is a 50% loss of helical content due to the interaction between the two systems. The time dependent variation of helicity further elicits that there are considerable changes in the helicity up to 8 ns. Afterward, variation in the helicity with time is only

**TABLE 2: Sequence of the SNARE Peptide Used in the Study Represented with Its Residue Number, Single Letter Code, and Their Respective Helix Adaptability in the Scale of 0–1<sup>a</sup>**

Res. No	2	3	4	5	6	7	8	9	10	11	12	13	14	15	16	17	18	19	20	21
Single Letter Code	D	A	R	E	N	E	M	D	E	N	L	E	Q	V	S	G	I	I	G	N
Helix propensity	0.69	0	0.21	0.4	0.65	0.4	0.24	0.69	0.4	0.65	0.21	0.4	0.39	0.61	0.5	1	0.41	0.41	1	0.65
Res. No	22	23	24	25	26	27	28	29	30	31	32	33	34	35	36	37	38	39	40	41
Single Letter Code	L	R	H	M	A	L	D	M	G	N	E	I	D	T	Q	N	R	Q	I	D
Helix propensity	0.21	0.21	0.61	0.24	0	0.21	0.69	0.24	1	0.65	0.4	0.41	0.69	0.66	0.39	0.65	0.21	0.39	0.41	0.69
Res. No	42	43	44	45	46	47	48	49	50	51	52	53	54	55	56	57	58	59	60	61
Single Letter Code	R	I	M	E	K	A	D	S	N	K	T	R	I	D	E	A	N	Q	R	A
Helix propensity	0.21	0.41	0.24	0.4	0.26	0	0.69	0.5	0.65	0.26	0.66	0.21	0.41	0.69	0.4	0	0.65	0.39	0.21	0

<sup>a</sup> The residues represented in red are uncoiled during the simulation and the residues represented in black retain the  $\alpha$ -helix structure during the simulation.

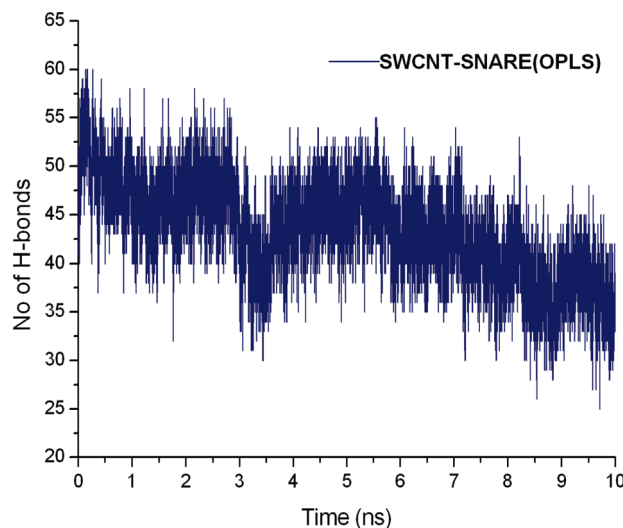


**Figure 13.** Number of H-bonds present in the SWCNT-SNARE(OPLS) systems during the simulation.

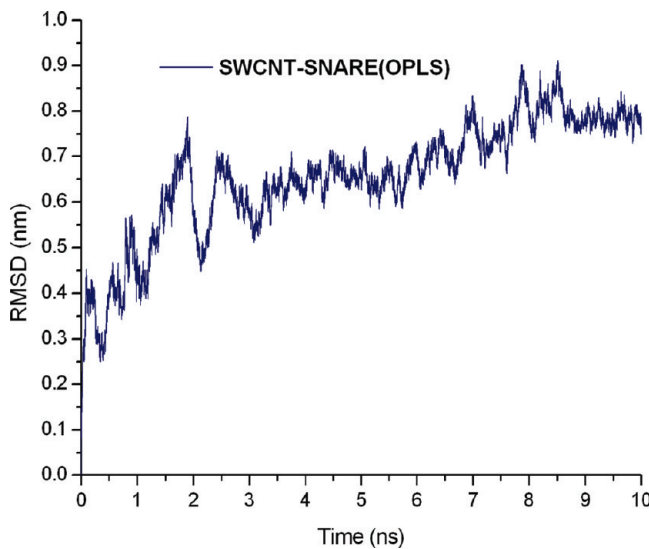


**Figure 14.** Root mean square deviation (RMSD) of the SWCNT-SNARE(OPLS) system with respect to its initial structure.

marginal. The changes in the number of H-bond present in the SNARE peptide with time is given in Figure 13. In concomitant with the changes in the helicity (50%), the decrease in the number of hydrogen bonds in the helix can be noticed.

The plot of RMSD with time is given Figure 14 for the SWCNT-SNARE (OPLS) system. It can be observed from the results that the RMSD of the SNARE increases up to 8 ns and thereafter changes are minimal. The number of clusters obtained for the SWCNT-SNARE (OPLS) system as a function of time is represented in Figure 15. The evolution of cluster terminates approximately around 2 ns. The structure of the SWCNT-SNARE (OPLS) complex obtained from the most dominant cluster is presented in the Figure 16, which delineates all the above-mentioned characteristic variations in the helix.

The plot of contact area between the SWCNT and SNARE with time is depicted in Figure 17. The fluctuation in the contact area attains saturation beyond 8 ns. It is observed that the variations in the maximum contact area range from 8 to 10 nm<sup>2</sup>, which are marginally higher than that of SWCNT-PA<sub>40</sub> (4–6 nm<sup>2</sup>). This may be due to the higher number of residues and the presence of longer side chain amino acids in the SNARE helix when compared to the presence of CH<sub>3</sub> group in the PA<sub>40</sub>.

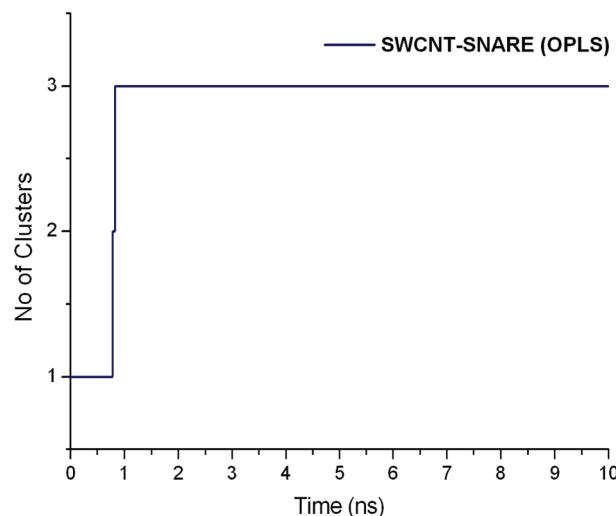


**Figure 15.** Number of clusters obtained for the SWCNT-SNARE system as a function of time.

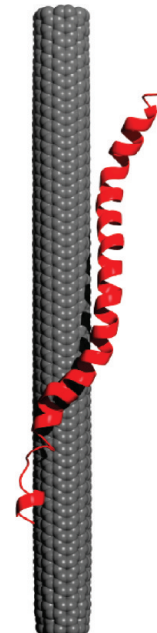


**Figure 16.** Structure of the most dominant cluster extracted from the simulation of SWCNT-SNARE(OPLS).

## 5. Conclusion

Different structural parameters obtained from the MD simulations on various systems reveal that PA<sub>40</sub> interacts with the surface of the SWCNT by expelling the water molecules. Furthermore, breakage of hydrogen bonds in the  $\alpha$ -helix is observed, which leads to conformational transitions ( $\alpha \rightarrow \text{turns}$ ) in different segments of PA<sub>40</sub>. As a consequence, regions of different structural and energetic stability are generated in PA<sub>40</sub> during the interaction and the structurally and energetically weaker regions curl around the surface of the SWCNT. The results observed from the various trajectories elucidate that the overall trend is not significantly influenced by the initial geometry. Both the parallel and angular orientations of helical fragment with respect to the SWCNT yield similar results. Although the finer details obtained from the MD simulation using ff03 and OPLS are different, the overall conclusion derived from ff03 is akin to that of OPLS.

Evidence from the interaction of the  $\alpha$ -helical fragment obtained from the SNARES protein shows that the conforma-

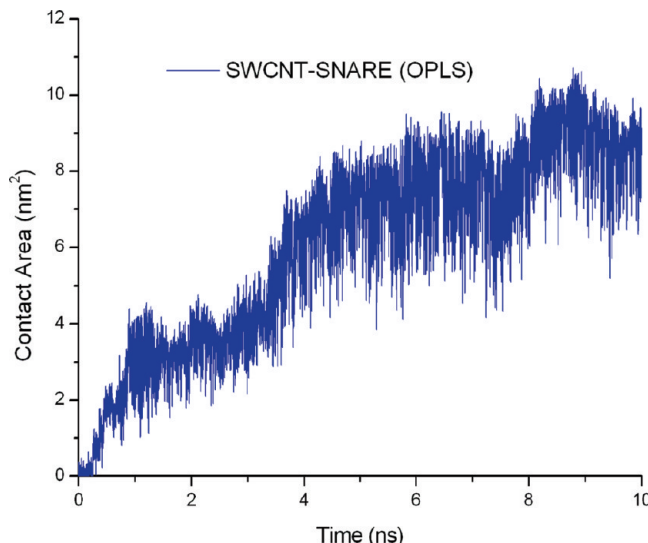


**Figure 17.** Contact area between the SWCNT-SNARE(OPLS) system as a function of time.

tional transition in  $\alpha$ -helix depends on the amino acid composition and sequence. In addition, it is found that the wrapping of an  $\alpha$ -helical fragment from the SNAREs is similar to that of the model PA<sub>40</sub>. In summary, a decrease in the  $\alpha$ -helical content is observed upon interaction with the SWCNT, which is in close agreement with the experimental results.

**Acknowledgment.** We thank the Board of Research in Nuclear sciences (BRNS), Mumbai, India, and Council of Scientific and Industrial Research (CSIR), New Delhi, India, for Financial Support. K.B thanks Dr. Robert R Johnson, Temple Institute for Computational Molecular Science, for useful discussions. We also thank Dr. C. N. Patra and Dr. S. K. Ghosh, BARC, for their valuable suggestions and comments and Dr. T. Ramasami, Secretary, DST, GOI, and Dr. A. B. Mandal, Director CLRI for their continued support.

## References and Notes

- Baughman, R. H.; Cui, C. X.; Zakhidov, A. A.; Iqbal, Z.; Barisci, J. N.; Spinks, G. M.; Wallace, G. G.; Mazzoldi, A.; De Rossi, D.; Rinzler, A. G.; Jaschinski, O.; Roth, S.; Kertesz, M. *Science* **1999**, 284, 1340.
- Sazonova, V.; Yaish, Y.; Ustunel, H.; Roundy, D.; Arias, T. A.; McEuen, P. L. *Nature* **2004**, 431, 284.
- Kong, J.; Franklin, N. R.; Zhou, C. W.; Chapline, M. G.; Peng, S.; Cho, K. J.; Dai, H. J. *Science* **2000**, 287, 622.
- Snow, E. S.; Perkins, F. K.; Houser, E. J.; Badescu, S. C.; Reinecke, T. L. *Science* **2005**, 307, 1942.
- Hinds, B. J.; Chopra, N.; Rantell, T.; news, R.; Gavalas, V.; Bachas, L. G. *Science* **2004**, 303, 62.
- Kalra, A.; Garde, S.; Hummer, G. *Proc. Natl. Acad. Sci. U.S.A.* **2003**, 100, 10175.
- Lin, Y.; Taylor, S.; Li, H. P.; Fernando, K. A. S.; Qu, L. W.; Wang, W.; Gu, L. R.; Zhou, B.; Sun, Y. P. *J. Mater. Chem.* **2004**, 14, 527–541.
- Katz, E.; Willner, I. *ChemPhysChem* **2004**, 5, 1085–1104.
- Lacerda, L.; Bianco, A.; Prato, M.; Kostarelos, K. *Adv. Drug Delivery Rev.* **2006**, 58, 1460–1470.
- Baughman, R. H.; Cui, C. X.; Zakhidov, A. A.; Iqbal, Z.; Barisci, J. N.; Spinks, G. M.; Wallace, G. G.; Mazzoldi, A.; De Rossi, D.; Rinzler, A. G.; Jaschinski, O.; Roth, S.; Kertesz, M. *Science* **1999**, 284, 1340–1344.
- Sandeep, S. K.; Alexey, A. V.; Ravi, S. K.; Jonathan, S. D. *Langmuir* **2004**, 20 (26), 11594–11599.
- Matsuura, K.; Saito, T.; Okazaki, T.; Ohshima, S.; Yumura, M.; Iijima, S. *Chem. Phys. Lett.* **2006**, 429, 497–502.
- Zhao, X.; Liu, R.; Chi, Z.; Teng, Y.; Qin, P. *J. Phys. Chem. B* **2010**, 114, 5625–5631.
- Chiu, C. C.; Dieckmann, G. R.; Nielsen, S. O. *J. Phys. Chem. B* **2008**, 112 (51), 16326–16333.
- Dieckmann, G. R.; Dalton, A. B.; Johnson, P. A.; Razal, J.; Chen, J.; Giordano, G. M.; Muñoz, E.; Musselman, I. H.; Baughman, R. H.; Draper, R. K. *J. Am. Chem. Soc.* **2003**, 125, 1770–1777.
- Vijayan, M.; Yathindra, N.; Kolaskar, S. A. *Perspectives in structural biology*; University Press: Hyderabad, India, 1999.
- Enkhbayar, P.; Hikichi, K.; Osaki, M.; Kretsinger, R. H.; Matsumura, N. *Proteins: Struct., Funct., Bioinf.* **2006**, 64, 691–699.
- Zagrovic, B.; Jayachandran, G.; Millett, I. S.; Doniach, S.; Pande, V. S. *J. Mol. Biol.* **2005**, 353, 232–241.
- Podtelezhnikov, A. A.; Wild, D. L. *Proteins: Struct., Funct., Bioinform.* **2005**, 61, 94–104.
- Job, G. E.; Kennedy, R. J.; Heitmann, B. R.; Miller, J. S.; Walker, S. M.; Kemp, D. S. *J. Am. Chem. Soc.* **2006**, 128, 8227–8233.
- Agostini, F. P.; Soares-Pinto, D. D.; Moret, M. A.; Osthoff, C.; Pascutti, P. G. *J. Comput. Chem.* **2006**, 27, 1142–1155.
- Djurđević, D. P.; Biggs, M. J. *J. Comput. Chem.* **2006**, 27, 1177–1195.
- Paschek, D.; Gnanakaran, S.; Garcia, A. E. *Proc. Natl. Acad. Sci. U.S.A.* **2005**, 102, 6765–6770.
- Parthasarathi, R.; Raman, S. S.; Subramanian, V.; Ramasami, T. *J. Phys. Chem. A* **2007**, 111, 7141–7148.
- Fiori, W. R.; Miick, S. M.; Millhauser, G. L. *Biochemistry* **1993**, 32, 11957–11962.
- Marqusee, S.; Robbins, V. H.; Baldwin, R. L. *Proc. Natl. Acad. Sci. U.S.A.* **1989**, 86, 5286–5290.
- Spek, E. J.; Olson, C. A.; Shi, Z.; Kallenbach, N. R. *J. Am. Chem. Soc.* **1999**, 121, 5571–5572.
- Kennedy, R. J.; Walker, S. M.; Kemp, D. S. *J. Am. Chem. Soc.* **2005**, 127, 16961–16968.
- Couch, V. A.; Cheng, N.; Nambiar, K.; Fink, W. *J. Phys. Chem. B* **2006**, 110, 3410–3419.
- Tanford, C. *The Hydrophobic Effect: Formation of Micelles and Biological Membranes*, 2nd ed.; Wiley-Interscience: London, U.K., 2000.
- Levy, Y.; Onuchic, J. N. *Annu. Rev. Biophys. Biomol. Struct.* **2006**, 35, 389.
- Ryu, J.-H.; Hong, D.-J.; Lee, M. *Chem. Commun.* **2008**, 1043.
- Oshovsky, G. V.; Reinoudt, D. N.; Verboom, W. *Angew. Chem., Int. Ed.* **2007**, 46, 2366.
- Pace, C. N.; Schotlz, J. M. *Biophys. J.* **1998**, 75, 422–427.
- Best, R. B.; Buchete, N. V.; Hummer, G. *Biophys. Lett.* **2008**, L07–L09.
- Wang, T.; Wade, R. C. *J. Chem. Theory. Comput.* **2006**, 2, 140–148.
- Best, R. B.; Hummer, G. *J. Phys. Chem. B* **2009**, 113, 9004–9015.
- Matthes, D.; De Groot, B. L. *Biophys. J.* **2009**, 97, 599–608.
- Karplus, M.; McCammon, J. A. *Nat. Struct. Biol.* **2002**, 9, 788.
- Karplus, M. *Biopolymers* **2003**, 68, 350–358.
- Karplus, M.; McCammon, J. A. *Nat. Struct. Biol.* **2002**, 9 (9), 646–652.
- Johnson, R. R.; Johnson, A. T. C.; Klein, M. L. *Nano Lett.* **2008**, 8 (1), 69–75.
- Johnson, R. R.; Kohlmeyer, A.; Johnson, A. T. C.; Klein, M. L. *Nano Lett.* **2009**, 9 (2), 537–541.
- Kang, Y. K.; Lee, O.; Deria, P.; Kim, S. H.; Park, T.; Bonnell, D. A.; Saven, J. G.; Therien, M. J. *Nano Lett.* **2009**, 9, 1414–1418.
- Chiu, C. C.; Dieckmann, G. R.; Nielsen, S. O. *Biopolymers (Pept. Sci.)* **2009**, 92, 156–163.
- Gianese, G.; Rosato, V.; Cleri, F.; Celino, M.; Morales, P. *J. Phys. Chem. B* **2009**, 113, 12105–12112.
- Toma'sio, M. S.; Walsh, R. T. *J. Phys. Chem. C* **2009**, 113, 8778–8785.
- Humphrey, W.; Dalke, A.; Schulten, K. *J. Mol. Graph.* **1996**, 14, 33–38.
- Hummer, G.; Rasaiah, J. C.; Noworyta, J. P. *Nature* **2001**, 414 (6860), 188–190.
- Jenness, G. R.; Jordan, K. D. *J. Phys. Chem. C* **2009**, 113 (23), 10242–10248.
- DeLano, W. L. *The PyMOL Molecular Graphics System*; DeLano Scientific LLC, Palo Alto, CA, 2008.
- Sutton, R. B.; Fasshauer, D.; Jahn, R.; Brunger, A. T. *Nature* **1998**, 395, 347–353.
- Duan, Y.; Wu, C.; Chowdhury, S.; Lee, M. C.; Xiong, G.; Zhang, W.; Yang, R.; Cieplak, P.; Luo, R.; Lee, T.; Caldwell, J.; Wang, J.; Kollman, P. A. *J. Comput. Chem.* **2003**, 24, 1999–2012.
- Kaminski, G.; Friesner, R.; Tirado-Rives, J.; Jorgensen, W. *J. Phys. Chem. B* **2001**, 105, 6474–6487.
- Jorgensen, W.; Maxwell, D.; Tirado-Rives, J. *J. Am. Chem. Soc.* **1996**, 118, 11225–11236.
- Berendsen, H. J. C.; Postma, J. P. M.; van Gunsteren, W. F.; Hermans, J. In *Simple Point Charge Water. In Intermolecular Forces*; Pullman, B., Ed.; Reidel: Dordrecht, The Netherlands, 1981.
- Berendsen, H. J. C.; van der Spoel, D.; van Drunen, R. *Comput. Phys. Commun.* **1995**, 91, 43–56.

- (58) Lindahl, E.; Hess, B.; van der Spoel, D. *J. Mol. Model.* **2001**, *7*, 306–317.
- (59) Hess, B.; Kutzner, C.; van der Spoel, D.; Lindahl, E. *J. Chem. Theory Comput.* **2008**, *4*, 435–447.
- (60) Sherrill, D. C.; Sumpter, B. G.; Sinnokrot, O. M.; Marshall, S. M.; Hohenstein, G. E.; Walker, R. C.; Gould, R. I. *J. Comput. Chem.* **2009**, *30*, 2187–2193.
- (61) Parrinello, M.; Rahman, A. *J. Appl. Phys.* **1981**, *52*, 7182–7190.
- (62) Nosé, S.; Klein, M. L. *Mol. Phys.* **1983**, *50*, 1055–1076.
- (63) Bussi, G.; Donadio, D.; Parrinello, M. *J. Chem. Phys.* **2007**, *126*, 14101–14107.
- (64) Darden, T.; York, D.; Pedersen, L. *J. Chem. Phys.* **1995**, *103*, 8577–8593.
- (65) Hess, B.; Bekker, H.; Benderson, H. J. C.; Fraaije, J. G. E. M. *J. Comput. Chem.* **1997**, *18*, 1463–1473.
- (66) Kabsch, W.; Sander, C. *Biopolymers* **1983**, *22*, 2577–2637.
- (67) Daura, X.; Gademann, K.; Jaun, B.; Seebach, D.; van Gunsteren, W. F.; Mark, A. E. *Angew. Chem., Int. Ed.* **1999**, *38*, 236–240.
- (68) Kumar, S.; Bansal, M. *Biophys. J.* **1998**, *75*, 1935–1944.

JP106177N